

Preparation of a self-cleanable molecularly imprinted sensor based on surface-enhanced Raman spectroscopy for selective detection of R6G

Hongji Li¹ · Zirun Wang² · Xiaonan Wang² · Jiaqi Jiang² · Yeqing Xu¹ · Xiqing Liu¹ · Yongsheng Yan^{1,3} · Chunxiang Li³

Received: 9 December 2016 / Revised: 5 May 2017 / Accepted: 11 May 2017 / Published online: 8 June 2017
© Springer-Verlag Berlin Heidelberg 2017

Abstract Novel molecularly imprinted polymers (MIPs) based on the technique of surface-enhanced Raman scattering (SERS) were successfully prepared. Firstly, ZnO nanorods were fabricated with Ag by reduction of Ag⁺ on the surface of the ZnO nanorods. Then, ZnO/Ag heterostructures were used as the substrate, rhodamine 6G was used as the template molecule, acrylamide was used as the functional monomer, ethylene glycol dimethacrylate was used as the cross-linker, and 2,2'-azobis(2-methylpropionitrile) was used as the initiator to prepare the ZnO/Ag MIPs (ZOA-MIPs). Through characterization analysis, it was proved that the novel ZOA-MIPs exhibited excellent SERS properties and selectivity. Under the optimal conditions, there was a good linear relationship ($R^2 = 0.996$) between the Raman signal (at 1654 cm⁻¹) and the concentration of the templates, and the detection limit was 10⁻¹³ mol L⁻¹. It was also proved that the ZOA-MIPs had the property of self-cleaning, resulting in good reusability. It is envisaged that the sensitivity of SERS coupled with the selectivity of MIPs could result in a promising chemosensor for practical applications.

Keywords Molecularly imprinted polymers · Surface-enhanced Raman scattering · ZnO/Ag heterostructures · Self-cleaning · Selective detection

Introduction

Noble metal nanoparticles (NPs) are candidate materials with unusual optical and electronic properties and are widely used in the fields of sensing, catalysis, and biomedicine [1–3]. Specially, numerous investigations have concentrated on Au and Ag NPs in spectroscopic analyses because of their intense visible-region absorption that can be largely attributed to surface plasmon resonance [4]. Surface-enhanced Raman scattering (SERS), as an attractive technique with high sensitivity, rapid response, and fingerprint management, has become one of the most valuable tools in nondestructive chemical and biochemical analysis, mainly because of its ultrahigh sensitivity and rich molecular structural information, and the tremendous multiplexing capabilities of Raman spectroscopy [5, 6]. The Raman signals of the probe molecules on or near the surface of metallic NPs can be markedly magnified more than 10⁸ times, which makes the SERS technique useful for sensitive detection and even single-molecule analysis [7–9]. Especially, Ag NPs have a stronger and more sensitive SERS signal than Au NPs, so they have better performance in plasmonic sensing and SERS applications [10, 11]. However, there are also containing major drawbacks in the use of metallic NPs as SERS substrates, such as the relatively low reusability and stability, especially when an aggregation agent is added to produce more hot spots for improvement of sensitivity [12]. Importantly, most of the SERS substrates cannot be easily cleaned and reused after SERS analyses. This is inconvenient and not cost-effective because of the high costs

Electronic supplementary material The online version of this article (doi:10.1007/s00216-017-0410-y) contains supplementary material, which is available to authorized users.

✉ Chunxiang Li
licxtougao@126.com

¹ School of Chemistry and Chemical Engineering, Jiangsu University, Zhenjiang, Jiangsu 212013, China

² School of Chemistry, Jilin Normal University, Siping, Jilin 136000, China

³ Institute of Green Chemistry and Chemical Technology, Jiangsu University, Zhenjiang, Jiangsu 212013, China

of noble metals. Therefore, it is important to prepare more effective substrates to broaden the application range of SERS.

Recently, some investigations have focused on assembly of metallic NPs growing on solid substrates such as glass slides, silicon wafers, and metal–semiconductor heterostructures [13–15] or even filter paper [16] to adjust the SERS activity of the substrates. On the one hand, this broadens traditional SERS detection applications, and on the other hand, several investigations have reported that when the metallic NPs contact with the metal–semiconductor heterostructures, the Raman signal will be significantly enhanced. For example, Ko et al. [17] prepared three-dimensional Al_2O_3 membranes loaded with Au NPs and explored the SERS enhancement. Zhao et al. [18] prepared anatase-phase TiO_2 nanofibers and subsequently surface decorated them with Ag NPs for use in 4-mercaptobenzoic acid detection [18]. It is considered that the increase of the evanescent field could be responsible for the SERS effect, which could result in significant enhancement at neck interconnections between associated NPs [19] or in metal–semiconductor heterostructures, resulting in specific metal–semiconductor interface interactions [20, 21]. Moreover, it has been proved from recent investigations that several metal–semiconductor heterostructures can also generate a weak SERS signal. For example, both TiO_2 and ZnO exhibited a prominent enhancement factor up to 1×10^3 [22, 23]. Importantly, the morphology of ZnO can be controlled easily, so it is widely used in SERS detection [24]. On the basis of these findings, it is considered that the formation of heterostructures by combination of metallic NPs with metal semiconductors could further promote the SERS effects of metallic NPs under the assistance of supporting electromagnetic enhancement from metal–semiconductor heterostructures [25–27]. However, the present design of SERS substrates is mostly focused on the preparation of SERS substrates and ignores the lack of specific selectivity for the target molecule of traditional substrate materials.

The molecular imprinting technique has been introduced into SERS detection to improve the selectivity of traditional SERS substrate materials. This technique can create molecularly imprinted polymers (MIPs) containing specific recognition cavities chemically complementary to the template molecules by a mimetic approach [28, 29]. Recently, some investigations into MIPs and SERS have been presented: For example, Hu et al. [30] prepared a novel biosensor combining MIPs and SERS to determine melamine in milk [30]. Kamra et al. [31] constructed MIP-based chemical sensors for nicotine detection by SERS. Although these methods have the excellent property of SERS detection, there have been few investigations into combining heterostructure SERS substrates with MIPs.

In this work, we firstly attempted to combine heterostructure SERS substrates with MIPs to improve the selectivity and use for the target (rhodamine 6G) analyte in water. Under the optimal conditions, R6G was selected as the template molecule, ZnO/Ag

was selected as the SERS substrate, acrylamide (AM) was selected as the functional monomer, and ethylene glycol dimethacrylate (EGDMA) was selected as the cross-linker to prepare highly sensitive ZnO/Ag R6G-imprinted MIPs (ZOA-MIPs) by precipitation polymerization. The ZOA-MIPs could selectively bind R6G and significantly enhance the Raman signal of the R6G. Moreover, the research indicated that the ZOA-MIPs also possessed the property of self-cleaning under UV light irradiation. The sensing strategy might provide an attractive and cost-effective approach to rapidly monitor R6G and various organic dyestuffs, and this technique could broaden the application range of SERS detection.

Experimental

Chemicals and materials

Silver nitrate, zinc chloride, AM, ethanolamine, methylbenzene, acetonitrile, and ethanol were purchased from Sinopharm Chemical Reagent Co. (Shanghai, China). γ -Methacryloxypropyl trimethoxysilane (MPS), EGDMA, polyvinylpyrrolidone (K30), ammonium hydroxide (28%), 2,2'-azobis(2-methylpropionitrile), R6G, rhodamine B (RB), and crystal violet (CV) were purchased from Aladdin Reagent Co. (Shanghai, China). Ultrapure water was used for preparation of all aqueous solutions and cleaning processes.

Apparatus and measurements

The surface morphology of the samples was detected by a scanning electron microscope (SEM; JEOL, JSM-7001 F). IR spectra ($4000\text{--}500\text{ cm}^{-1}$) were collected with a NEXUS-470 Fourier transform IR apparatus (Nicolet, USA) with use of KBr disks. UV–visible (UV–vis) absorption spectra were obtained with a UV–vis spectrophotometer (UV-2450, Shimadzu, Japan). During the photocatalytic processes, a 15-W mercury lamp with maximum emission at 365 nm was used as the UV light source. The thermogravimetric analyses (TGA) of samples were performed with a Diamond TGA/differential thermal analysis instrument (STA 449C Jupiter, Netzsch, Germany) under a nitrogen atmosphere up to $800\text{ }^\circ\text{C}$ with a heating rate of $5.0\text{ }^\circ\text{C min}^{-1}$. The X-ray diffraction (XRD) spectra were collected with an XRD-6100 Lab X-ray diffractometer (Shimadzu, Japan) with $\text{Cu K}\alpha$ radiation over the 2θ range of $20\text{--}80^\circ$. Raman spectra were obtained with a confocal micro Raman spectroscopy system (Renishaw INVIA, Germany).

Synthesis of ZnO nanorod powder

The synthesis of ZnO nanorods (NRs) was according to the process in the literature with minor modifications [32].

Generally, 1.0 g ZnCl₂ was dispersed in 70 mL ultrapure water at room temperature and mixed ultrasonically for 15 min, and then 5.0 mL ammonium hydroxide was dropped into the mixture under stirring. The mixture was transferred into a 100-mL Teflon autoclave and kept at 150 °C for 3.0 h. Finally, the products were collected by centrifugation and repeatedly washed with water and ethanol three times to remove the unreacted reagent. The final products were dried in a vacuum at room temperature and sealed for further use.

Synthesis of ZnO/Ag heterostructures

The ZnO/Ag heterostructures were prepared by the sol-gel method by reduction of Ag on the surface of ZnO NRs. Generally, 100 mg ZnO NRs was dispersed in 50 mL of a solution of ethanol and water (4:1, v/v), and 2.0 mL AgNO₃ (0.1 mol L⁻¹) and 5.0 mL polyvinylpyrrolidone (0.2 mol L⁻¹) were added to the solution, and the solution was stirred magnetically in the dark for 4.0 h. Then, 300 µL ethanolamine was added to the mixture, and the temperature was raised to 50 °C for another 12 h. The ZnO/Ag heterostructures obtained were collected by centrifugation and repeatedly washed with water and ethanol three times to remove the unreacted reagent. The final products were dried in a vacuum at room temperature and sealed for further use.

Synthesis of ZOA-MIPs

Firstly, the ZnO/Ag heterostructures were decorated with vinyl groups via modification with MPS. Generally, 1.0 g ZnO/Ag heterostructures was dispersed in 50 mL anhydrous methylbenzene, and 1.0 mL MPS was added to the mixture under N₂ protection at 90 °C. After 12 h, the products were collected by centrifugation and washed with ethanol three times to remove the unreacted reagent. The final products were dried in a vacuum at room temperature and sealed for further use.

Secondly, the ZOA-MIPs were prepared by the method of precipitation polymerization, which used R6G as the template molecule, AM as the functional monomer, EGDMA as the cross-linking agent, and 2,2'-azobis(2-methylpropionitrile) as the initiator. Briefly, 100 mg MPS-modified ZnO/Ag heterostructures was fully dispersed in 60 mL acetonitrile by ultrasonic mixing. Then, 0.1 mmol R6G, 0.4 mmol AM, and 2.0 mmol EGDMA were added to the solution at room temperature, and the solution was purged with N₂ for 10 min to thoroughly exhaust the oxygen. Finally, 10 mg 2,2'-azobis(2-methylpropionitrile) was added, and the mixture was sealed and put in a constant-temperature bath oscillator for two-step polymerization. Firstly, the reaction temperature was set at 50 °C for 6.0 h for prepolymerization. Secondly, the reaction temperature was raised to 60 °C for 24 h for polymerization. The products were collected by centrifugation and washed

with ethanol several times to remove the unreacted reagent. The templates were removed by further washing with a mixture of methanol and acetic acid (9:1, v/v) with Soxhlet extraction.

ZnO/Ag nonimprinted polymers (ZOA-NIPs) that had no R6G were prepared for a comparison test.

Binding experiment

It was believed that the SERS detection property of ZOA-MIPs was influenced by the capacity of binding to the templates, and the binding capacity was obtained from the adsorption experiment. Briefly, at room temperature, 10 mg ZOA-MIPs or 10 mg ZOA-NIPs was added to a 20 mg L⁻¹ R6G solution. Then the solution was transferred to a thermostat with a temperature of 25 °C for incubation for 12 h, and the supernatant was detected by the UV-vis spectrophotometer to determine the residual R6G. The adsorption efficiency was calculated according to the following equation:

$$E = \frac{C_0 - C}{C_0} \times 100\% \quad (1)$$

This equation reflects the adsorption effect of the ZOA-MIPs and ZOA-NIPs with regard to R6G. In the equation, *E* is the adsorption efficiency of ZOA-MIPs or ZOA-NIPs, and *C*₀ and *C* are the initial and equilibrium concentrations of R6G respectively.

Furthermore, to investigate the selective properties of ZOA-MIPs, RB and CV were chosen as the interferent, and the ZOA-MIPs and ZOA-NIPs were chosen as the adsorbent. The adsorption test was similar to that for the adsorption of R6G.

Raman detection measurement

The SERS detection capability of the ZOA-MIPs was reflected by Raman spectra. In this experiment, all the Raman detections were under uniform conditions: the excitation wavelength was 633 nm. The spectra of each sample were collected with an exposure time of 10 s and an incident laser power of 0.25 mW. SERS spectra were collected with a × 50 Nikon objective. All the SERS substrates were dropped on a glass slide and naturally dried before SERS detection.

Results and discussion

Preparation and characterization of ZOA-MIPs

The ZOA-MIPs were prepared through a multistep procedure (Fig. 1). As shown in Fig. 1, the ZnO NRs were synthesized by a hydrothermal reaction. The -OH groups on the surface of

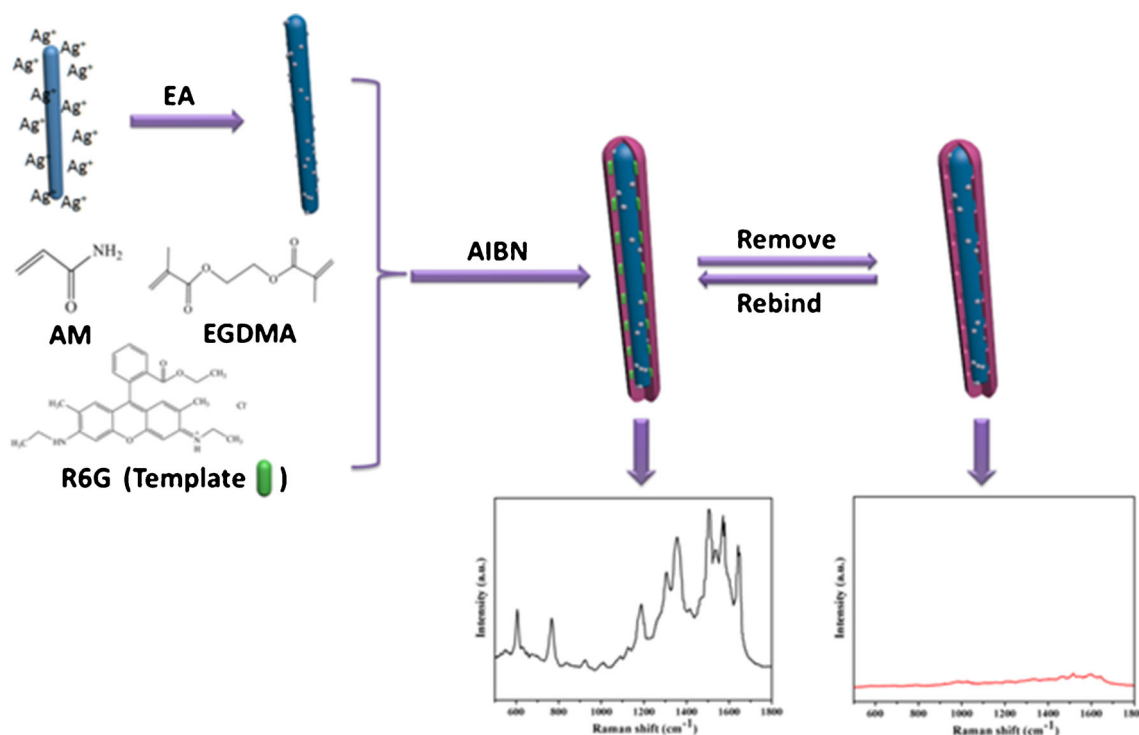


Fig. 1 Preparation of the ZnO/Ag molecularly imprinted polymers (ZOA-MIPs) and the surface-enhance Raman scattering (SERS) detection of rhodamine 6G (*R6G*) on specific recognition. *AIBN* 2,2'-

azobis(2-methylpropionitrile), *AM* acrylamide, *EA* ethanolamine, *EGDMA* ethylene glycol dimethacrylate

ZnO NRs acted as active sites for adsorption of Ag^+ ions. Then, Ag NPs were restored and anchored on the surface of the ZnO NRs by the sol-gel reaction with the assistance of ethanolamine. Next, the ZnO/Ag heterostructures were modified by MPS. Finally, the copolymerization of the vinyl-modified ZnO/Ag heterostructures (substrate materials), AM (functional monomer), R6G (template molecules), and EGDMA (cross-linking agent) was performed. ZOA-MIPs that possess specific recognition cavities were obtained when the embedded template molecules were removed.

As shown in Fig. 2, to study the applicability of this polymerization method, the morphology of the synthesized materials was observed with an SEM. Cylindrical ZnO NRs with a smooth surface were successfully produced. The NR size distribution was narrowed to 2 μm in length (Fig. 2a). The

morphology of ZnO/Ag heterostructures is shown in Fig. 2b. The AgNPs were scattered on the surface of ZnO nanorods and all of the Ag nanoparticles are modified on the surface of ZnO nanorods. It was evident that adjacent Ag NPs were separated by a nanoscale distance and the interparticle gaps would lead to the generation of Raman “hot spots,” which could substantially enhance the local electromagnetic fields, resulting in enormously strong SERS activity [33, 34]. The morphology of the ZOA-MIPs is shown in Fig. 2c. There were no obvious changes in the surface morphology of ZnO/Ag heterostructures and ZOA-MIPs except for a small amount of scattering aggregates, which were possibly the reason for self-polymerization of functional monomers.

Figure 3 shows the Fourier transform IR spectra of ZOA-MIPs (curve a) and ZOA-NIPs (curve b). Both materials

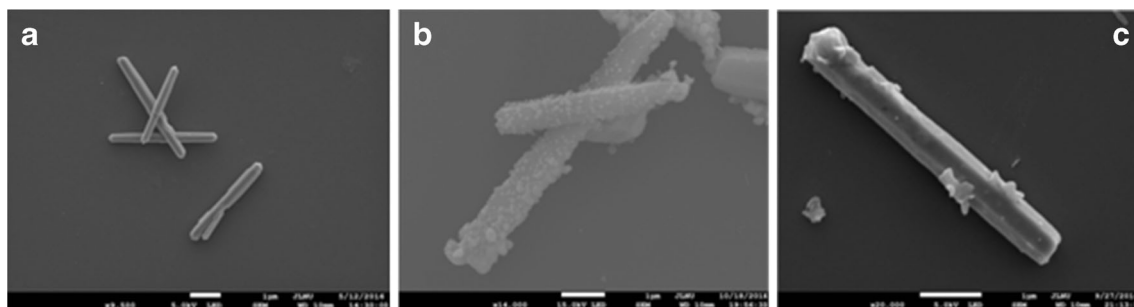


Fig. 2 Scanning electron microscope images of the synthesized material: ZnO nanorods (a), ZnO/Ag heterostructures (b) and ZOA-MIPs (c). Scale bars 1 μm

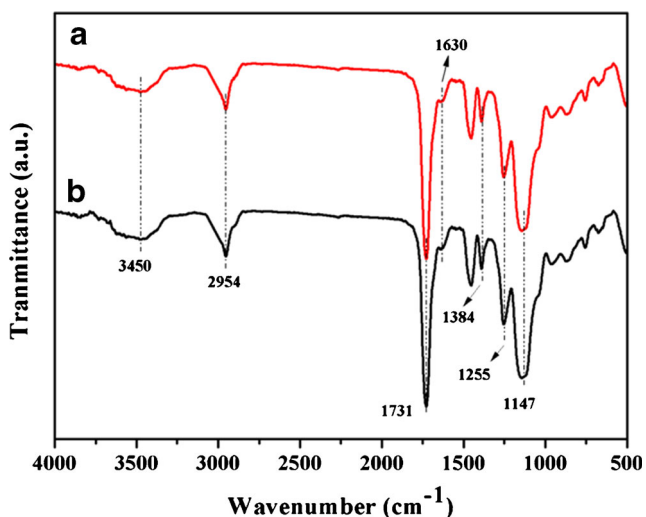


Fig. 3 Fourier transform IR spectra of ZOA-MIPs (a) and ZnO/Ag nonimprinted polymers (ZOA-NIPs; b)

presented obvious peaks, and they were at similar locations. The characteristic peaks at 1384 cm^{-1} , 1630 cm^{-1} , and 3450 cm^{-1} were attributed to the C–N stretch of the functional monomer (AM) and the stretching and bending vibrations of secondary amine groups of AM respectively [35]. The characteristic peaks at 1147 cm^{-1} , 1255 cm^{-1} (C–O–C stretching), and 1731 cm^{-1} (C=O stretching) were attributed to the cross-linker (EGDMA) [36]. The peak at 2954 cm^{-1} was responsible for the aliphatic C–H stretching vibrations. It was proved from the results that the polymerization was successfully initiated and the ZOA-MIPs and ZOA-NIPs were successfully prepared.

XRD patterns were used to analyze the synthesized materials (Fig. 4). The XRD pattern acquired from ZnO NRs (curve a) had strong diffraction peaks centered at the (100), (002), (101), (102), (110), (103), (112), and (202) crystal planes. The XRD pattern of ZnO/Ag heterostructures (curve

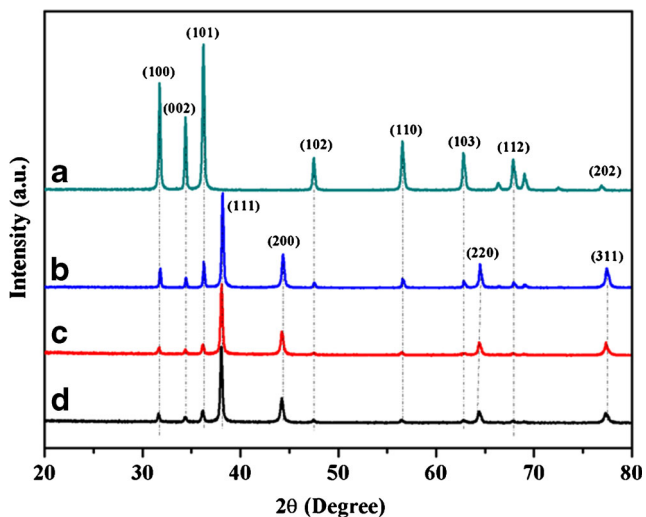


Fig. 4 X-ray diffraction patterns of ZnO (a), ZnO/Ag heterostructures (b), ZOA-MIPs (c), and ZOA-NIPs (d)

b) presented four additional diffraction peaks centered at (111), (200), (220), and (311), which were contributed by the crystallographic planes of the cubic crystal structure of elemental silver [37]. The relative intensity ratio and position of the diffraction peaks of ZOA-MIPs (curve c) and ZOA-NIPs (curve d) were almost identical, except the corresponding peak intensities were relatively weaker than those of ZnO/Ag heterostructures, indicating that the encapsulation process reduced the intensity of the diffraction peaks. The XRD results further proved the successful preparation of ZnO NRs, ZnO/Ag heterostructures, ZOA-MIPs, and ZOA-NIPs, and such results qualitatively agreed with those acquired from SEM analyses (Fig. 2).

TGA was performed to further prove the surface of ZnO/Ag heterostructures had been successfully coated with imprinted polymers. As shown in Fig. 5, the TGA of ZOA-MIPs was performed from room temperature to 800 °C . The first mass decrease stage occurred from room temperature to 150 °C , with a mass loss of 2.456% for ZOA-MIPs, which may due to the dehydration of the water residues or degasification of the gas absorbed in the polymer. The obvious mass loss (75.288%) in the second stage was from 150 to 490 °C , which was mainly caused by the loss of imprinted polymers. The mass remained relatively stable for the rest of the analysis from 450 to 800 °C . It was considered that the remnant was contributed by the more thermally resistant ZnO/Ag heterostructures, and the encapsulation efficiency of ZnO/Ag heterostructures in the MIPs was 4.911%. On the basis of these findings, it was proved that the ZOA-MIPs were successfully prepared.

Moreover, it was also very important that the templates (R6G) be thoroughly rinsed from the MIPs because the trace R6G could cause the Raman signal to change significantly. Firstly, the UV–vis spectrophotometer was used to monitor the concentration of R6G in the washing solution. As shown in Fig. S1a, the absorption peak gradually declined as the

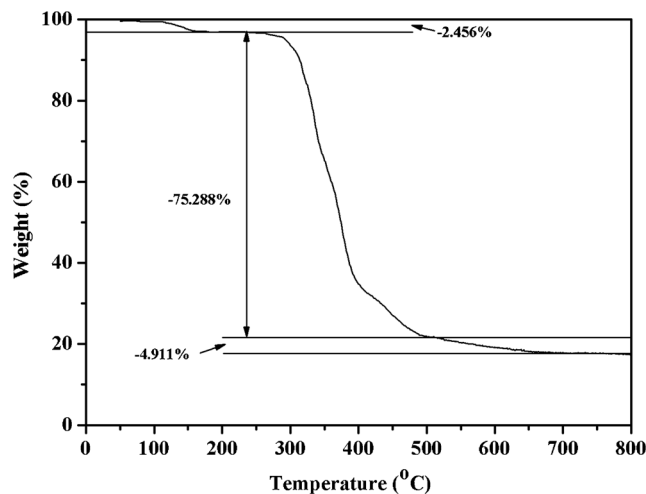


Fig. 5 Thermogravimetric analyses of the ZOA-MIPs

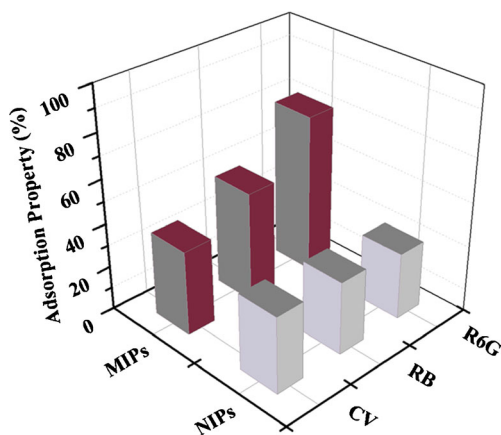


Fig. 6 The selective adsorption properties of ZOA-MIPs and ZOA-NIPs with regard to different molecules. CV crystal violet, RB rhodamine B

washing time increased. When the rinsing time exceeded 7 days, the absorption peak completely disappeared. Secondly, the Raman spectrometer was used to detect the concentration of R6G in the rinsing solution. The Raman spectra are shown in Fig. S1b, and the Raman intensities nearly disappeared after rinsing for 7 days. From the UV–vis absorption spectra and the Raman spectra, it was proved that the R6G that had been adsorbed on the MIPs had been thoroughly eliminated after rinsing for 7 days.

Adsorption properties of ZOA-MIPs

It is known that the adsorption properties reflect the binding affinity and selectivity of MIP materials, so adsorption experiments on ZOA-MIPs and ZOA-NIPs were performed with the UV–vis spectrophotometer. As shown in Fig. 6, under the optimal conditions, the adsorption capacities of ZOA-MIPs and ZOA-NIPs were 71.23% and 30.26% respectively. Moreover, the adsorption capacity of ZOA-MIPs for RB and CV were less than that for R6G, but the adsorption capacity of ZOA-NIPs for RB and CV was almost similar to that for R6G. This proved that the specific recognition cavities were important to ZOA-MIPs in the template selectivity and they could result in specific adsorption to R6G.

Determination of different concentrations of R6G in water by SERS

As shown in Fig. 7a, to check the SERS activity of the ZOA-MIPs, R6G was selected as the probe molecule to ascertain the limit of detection. The figure shows that the SERS intensity at 1654 cm^{-1} was the most distinct (the SERS spectra were collected with a $\times 50$ Nikon objective). Moreover, according to the literature [38], the observed peak at 1654 cm^{-1} can be attributed to symmetric modes of in-plane C–C stretching vibrations, so the band at 1654 cm^{-1} was assigned as the characteristic peak. From the figure, it is seen that the Raman

signals changed with different concentrations of R6G from 10^{-14} to $10^{-7}\text{ mol L}^{-1}$ on the as-prepared samples. The intensity of the characteristic peak at 1654 cm^{-1} gradually weakened but was still relatively intense with the concentration of R6G decreasing until $10^{-14}\text{ mol L}^{-1}$. When the concentration was $10^{-14}\text{ mol L}^{-1}$, the Raman signal almost disappeared. Therefore, the detection limit of ZOA-MIPs was considered to be $10^{-13}\text{ mol L}^{-1}$. Furthermore, as shown in Fig. 7b, there was a linear relationship between the intensity variation of the characteristic peak and the concentration of R6G between 10^{-11} and $10^{-7}\text{ mol L}^{-1}$; the coefficient of determination (R^2) of this regression model was 0.996. Below $10^{-11}\text{ mol L}^{-1}$, the calibration reached a plateau point. It was considered that the ZOA-MIPs could not effectively adsorb the templates when the concentration of the templates was extremely low, so they could not cause the Raman signal to change significantly. The enhancement factor

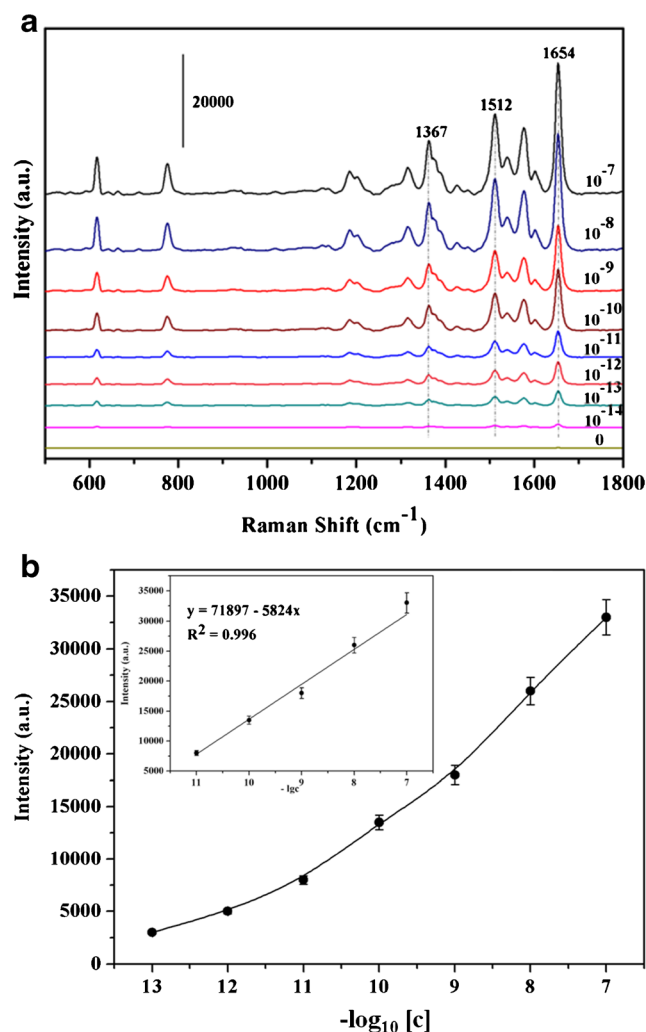


Fig. 7 a SERS spectra of different concentrations of R6G obtained from ZOA-MIPs. b The Raman intensity of the peak of 1654 cm^{-1} as a function of the R6G concentration for the concentration range from 10^{-13} to $10^{-7}\text{ mol L}^{-1}$, and the linear relation for the concentration range from 10^{-11} to $10^{-7}\text{ mol L}^{-1}$ (insert)

was calculated to be about $3.3 \times 10^{5-6}$ with use of the the R6G peak at 1654 cm^{-1} according to the following equation:

$$EF = \frac{I_{\text{SERS}}/N_{\text{SERS}}}{I_0/N_0} \quad (2)$$

In this equation, I_{SERS} and I_0 are the peak intensities of limit SERS detection and normal Raman detection at the same band respectively, and N_{SERS} and N_0 are the number of molecules in the focused incident laser spot in each of the two types of measurements.

As a contrast, the ZnO NRs, Ag NPs (prepared as in the synthesis of ZnO/Ag heterostructures but without addition of ZnO NRs), and ZnO/Ag heterostructures were used to detect R6G, but all of the effects were weaker than with ZOA-MIPs, and the detection limits of ZnO NRs, Ag NPs, and ZnO/Ag heterostructures were $10^{-3} \text{ mol L}^{-1}$, $10^{-7} \text{ mol L}^{-1}$, and $10^{-8} \text{ mol L}^{-1}$ respectively (see Fig. S2).

Selectivity and regeneration test

To investigate the specific selectivity of the ZOA-MIPs for R6G detection, molecules similar to R6G in structure (RB and CV) were examined by parallel assays with a concentration of $10^{-7} \text{ mol L}^{-1}$. As shown in Fig. 8, only feeble SERS intensities were observed for the comparative molecules because their structure did not match well with the specific recognition cavities, so they could not be effectively bound to the ZOA-MIPs. The Raman intensity of RB was a little stronger than that of CV, which indicated that the recognition cavities formed in the preparation of ZOA-MIPs could match with the templates in shape, size, and functional groups [39]. It can be seen from Fig S3 that RB is similar to R6G in structure, so the Raman intensity changed more significantly than that of CV. Furthermore, as a contrast, ZnO/Ag was used to detect the

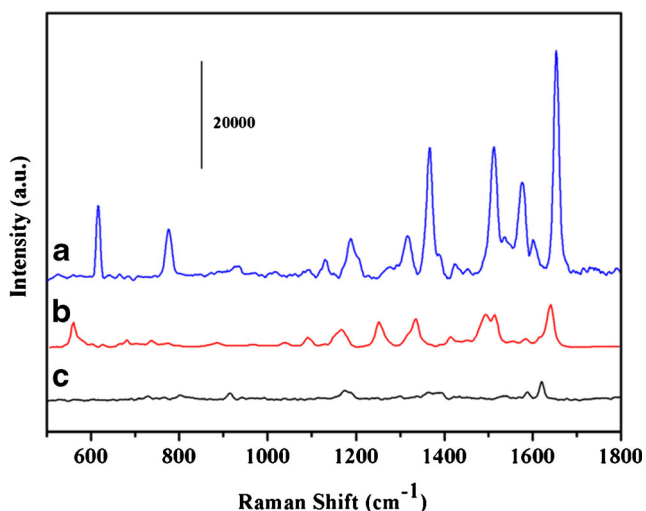


Fig. 8 SERS spectra of R6G (a), RB (b), and CV (c) recorded from ZOA-MIPs at the same concentration of 10^{-7} M

R6G molecules and the comparative molecules. From Fig. S4, it is seen that all the Raman signals of these molecules were almost the same intensity. This phenomenon was rationalized by the recognition cavities in the polymer layer effectively “capturing” the templates.

The traditional SERS sensors cannot be used more than once, so the detection effect of the SERS sensors is restricted. There was an urgent need of a method to fabricate a recyclable SERS sensor to be used in R6G detection. The materials prepared in this work not only possessed the function of detection but also has the property of self-cleaning. As shown in Fig. S5, the photocatalytic activity of the fabricated SERS substrate for the degradation of R6G under UV light irradiation was investigated. It was shown that the materials had the property of photocatalytic activity. As shown in Fig. S6, through adequate photodegradation and rinsing processes, none of the templates could be detected from the SERS substrates. It was proved that the templates were completely removed from the surface of ZOA-MIPs. Furthermore, it was also found that over five cycles of surface regeneration experiment, the SERS intensity of the peak at 1654 cm^{-1} for R6G varied by less than 8%. The results proved that the ZOA-MIPs could be regenerated and repeatedly used in R6G detection.

The mechanism of SERS detection

It is widely considered that the SERS detection mechanism is caused by two modes: electromagnetic enhancement (also called physical enhancement) and charge transfer (also called chemical enhancement). In this work, when the pure ZnO/Ag heterostructures were used as the substrate, the detection mechanism was regarded as electromagnetic enhancement. There were gaps between Ag NPs or Ag NPs and ZnO NRs, and these could have produced the “hot spots.” Meanwhile, the electromagnetic enhancement occurred in these regions of “hot spots.” But in this work, the ZOA-MIPs contained an imprinted layer on the surface of ZnO/Ag heterostructures, but also had the property of SERS, which could not be explained only with the traditional mechanism [40]. They may contain a special tunnel in the imprinted layer that could permit the template molecules through the imprinted shell to approach the surface of the substrates. The phenomenon was called a “gate effect” [41, 42], and Guo et al. [43] also proved the theory. Therefore, in this work, the templates (R6G) could through the imprinted layer approach surface of substrates and cause the Raman signal enhancement by electromagnetic enhancement.

Conclusions

In summary, ZnO NRs of about $1 \mu\text{m}$ were successfully prepared and were surface decorated with Ag NPs via a reduction

reaction. Then the ZnO/Ag heterostructures were used as the SERS substrates and coated with a layer of MIPs to be used in R6G detection. It was proved that the ZOA-MIPs had high sensitivity and selectivity for R6G. Moreover, the SERS sensor featured good self-cleaning and recyclability because of the excellent degradation ability of the ZnO/Ag. It is envisaged that the ZOA-MIPs are a kind of perfect SERS sensors and could be used in the detection of R6G or other organic dyestuffs in the environment.

Acknowledgements This work was financially supported by the National Natural Science Foundation of China (nos 21277063, 21407057, 21407064, 21507045, and 21576111), the National Basic Research Program of China (973 Program, 2012CB821500), the Natural Science Foundation of Jiangsu Province (nos BK20140534 and BK20140535), the National Postdoctoral Science Foundation (no. 2014 M561595), and the Postdoctoral Science Foundation funded project of Jiangsu Province (no. 1401108C).

Compliance with ethical standards

Conflict of interest The authors declare that they have no potential conflict of interest.

References

- Li HJ, Wei X, Zhang YF, Xu YQ, Lu K, Li CX, et al. Rapid and sensitive detection of hemoglobin with gold nanoparticles based fluorescence sensor in aqueous solution. *J Alloys Compd.* 2016;685:820–7.
- Qu YQ, Cheng R, Su Q, Duan XF. Plasmonic Enhancements of photocatalytic activity of Pt/N-Si/Ag photodiodes using Au/Ag core/shell nanorods. *J Am Chem Soc.* 2011;133:16730–3.
- Rycenga M, Cogley CM, Zeng J, Li W, Moran CH, Zhang Q, et al. Controlling the synthesis and assembly of silver nanostructures for plasmonic applications. *Chem Rev.* 2011;111:3669–712.
- Huang X, Jain PK, El-Sayed IH, El-Sayed MA. Gold Nanoparticles: interesting optical properties and recent applications in cancer diagnostics and therapy. *Nanomedicine.* 2007;2:681–93.
- Fang Y, Seong NH, Dlott DD. Measurement of the distribution of site enhancements in surface-enhanced Raman scattering. *Science.* 2008;321:388–92.
- Wang YQ, Yan B, Chen LX. SERS tags novel optical nanoprobe for bioanalysis. *Chem Rev.* 2013;113:1391–428.
- Chen JM, Huang YJ, Kannan PL, Zhang L, Lin ZY, Zhang JW, et al. Flexible and adhesive surface enhance Raman scattering active tape for rapid detection of pesticide residues in fruits and vegetables. *Anal Chem.* 2016;88:2149–55.
- Hossain MK, Kitahama Y, Huang GG, Han X, Ozaki Y. Surface-enhanced Raman scattering: realization of localized surface plasmon resonance using unique substrates and methods. *Anal Bioanal Chem.* 2009;394:1747–60.
- Li JF, Huang YF, Ding Y, Yang ZL, Li SB, Zhou XS, et al. Shell-isolated nanoparticle-enhanced Raman spectroscopy. *Nature.* 2010;464:392–5.
- Gutés A, Carraro C, Maboudian R. Silver Dendrites from galvanic displacement on commercial aluminum foil as an effective SERS substrate. *J Am Chem Soc.* 2010;132:1476–7.
- Wang L, Li H, Tian J, Sun X. Monodisperse, micrometer-scale, highly crystalline, nanotextured ag dendrites: rapid, largescale, wet-chemical synthesis and their application as SERS substrates. *ACS Appl Mater Interfaces.* 2010;2:2987–91.
- Ko H, Chang S, Tsukruk VV. Porous substrates for label free molecular level detection of nonresonant organic molecules. *ACS Nano.* 2009;3:181–8.
- Camden JP, Dieringer JA, Zhao J, Van Duyne RP. Controlled plasmonic nanostructures for surface-enhanced spectroscopy and sensing. *Acc Chem Res.* 2008;41:1653–61.
- Wu Y, Dong N, Fu S, Fowlkes JD, Kondic L, Vincenti MA, et al. Directed liquid phase assembly of highly ordered metallic nanoparticle arrays. *ACS Appl Mater Interfaces.* 2014;6:5835–43.
- Yang L, Yan B, Premasiri WR, Ziegler LD, Negro LD, Reinhard BM. Engineering nanoparticle cluster arrays for bacterial biosensing: the role of the building block in multiscale SERS substrates. *Adv Funct Mater.* 2010;20:2619–28.
- Zhou W, Yin BC, Ye BC. Highly sensitive surface-enhanced Raman scattering detection of hexavalent chromium based on hollow sea urchin-like TiO₂@Ag nanoparticle substrate. *Biosens Bioelectron.* 2017;87:187–94.
- Ko H, Chang S, Tsukruk VV. Porous substrates for label free molecular level detection of nonresonant organic molecules. *ACS Nano* 2009;3:181–188.
- Zhao Y, Sun L, Xi M, Feng Q, Jiang CY, Fong H. Electrospun TiO₂ nanofelt surface-decorated with Ag nanoparticles as sensitive and UV-cleanable substrate for surface enhanced Raman scattering. *ACS Appl Mater Interfaces.* 2014;6:5759–67.
- Tang H, Meng G, Huang Q, Zhang Z, Huang Z, Zhu C. Arrays of cone-shaped ZnO nanorods decorated with Ag nanoparticles as 3D surface-enhanced Raman scattering substrates for rapid detection of trace polychlorinated biphenyls. *Adv Funct Mater.* 2012;22:218–24.
- Chen T, Xing GZ, Zhang Z, Chen HY, Wu T. Tailoring the photoluminescence of ZnO nanowires using Au nanoparticles. *Nanotechnology.* 2008;19:17030–1.
- Zang Y, He X, Li J, Yin J, Li K, Yue C, et al. Band edge emission enhancement by quadrupole surface plasmon-exciton coupling using direct-contact Ag/ZnO nanospheres. *Nanoscale.* 2013;5:574–80.
- Jiang X, Li XL, Jia XF, Li GZ, Wang X, Wang GY, et al. Surface-enhanced Raman scattering from synergistic contribution of metal and semiconductor in TiO₂/MBA/Ag(Au) and Ag(Au)/MBA/TiO₂ assemblies. *J Phys Chem C.* 2012;116:14650–5.
- Wang H, Ruan W, Zhang J, Yang B, Xu W, Zhao B, et al. Direct observation of surface-enhanced Raman scattering in ZnO nanocrystals. *J Raman Spectrosc.* 2009;40:1072–7.
- Macias-Montero M, Borrás A, Saghi Z, Espinos JP, Barranco A, Cotrino J, et al. Vertical and tilted AgNPs@ZnO nanorods by plasma-enhanced chemical vapour deposition. *Nanotechnology.* 2012;23:255–303.
- Morton SM, Jensen L. Understanding the molecule-surface chemical coupling in SERS. *J Am Chem Soc.* 2009;131:4090–8.
- Zhang B, Wang H, Lu L, Ai K, Zhang G, Cheng X. Large-area silver-coated silicon nanowire arrays for molecular sensing using surface-enhanced Raman spectroscopy. *J Adv Funct Mater.* 2008;18:2348–55.
- Cheng C, Yan B, Wang SM, Li X, Zhou W, Yu T, et al. Fabrication and SERS performance of silver-nanoparticle decorated Si/ZnO nanotrees in ordered arrays. *J ACS Appl Mater Interfaces.* 2010;2:1824–8.
- Li SJ, Ge Y, Piletsky SA, Turner APF. A zipper-like on/off-switchable molecularly imprinted polymer. *J Adv Funct Mater.* 2011;21:3344–9.
- Wu YL, Yan M, Cui JY, Yan YS, Li CX. A Multiple-functional Ag/SiO₂/organic based biomimetic nanocomposite membrane for high-stability protein recognition and cell adhesion/detachment. *J Adv Funct Mater.* 2015;25:5823–32.

30. Hu Y, Feng SL, Gao F, Eunice CY, Li C, Grant E, et al. Detection of melamine in milk using molecularly imprinted polymers-surface enhanced Raman spectroscopy. *J Food Chem.* 2014;176:123–9.
31. Kamra T, Zhou TC, Montelius L, Schnadt J, Ye L. Implementation of molecularly imprinted polymer beads for surface enhanced Raman detection. *J Anal Chem.* 2015;87:5056–61.
32. Kim J, Yong KJ. Mechanism study of ZnO nanorod-bundle sensors for H₂S gas sensing. *J Phys Chem C.* 2011;115:7218–24.
33. Hao E, Schatz GC. Electromagnetic fields around silver nanoparticles and dimers. *J Chem Phys.* 2004;120:357–66.
34. Canamares MV, GarciaRamos JV, GomezVarga JD, Domingo C, SanchezCortes S. Comparative study of the morphology, aggregation, adherence to glass, and surface-enhanced Raman scattering activity of silver nanoparticles prepared by chemical reduction of Ag⁺ using citrate and hydroxylamine. *Langmuir.* 2005;21:8546–53.
35. Gao L, Li XY, Zhang Q, Dai JD, Wei X, Song ZL, et al. Molecularly imprinted polymer microspheres for optical measurement of ultra trace nonfluorescent cyhalothrin in honey. *J Food Chem.* 2014;156:1–6.
36. Yoshimatsu K, Reimhult K, Krozer A, Mosbach K, Sode K, Ye L. Uniform molecularly imprinted microspheres and nanoparticles prepared by precipitation polymerization: the control of particle size suitable for different analytical applications. *J Anal Chim Acta.* 2007;584:112–21.
37. Barakat N, Woo AM, Kanjwal KD, Choi MA, Khil KE, Kim MS. Surface plasmon resonances, optical properties, and electrical conductivity thermal hysteresis of silver nanofibers produced by the electrospinning technique. *Langmuir J Am Chem Soc.* 2008;24:11982–7.
38. Tang H, Meng G, Huang Q, Zhang Z, Huang Z, Zhu C. Arrays of cone-shaped ZnO nanorods decorated with Ag nanoparticles as 3D surface-enhanced Raman scattering substrates for rapid detection of trace polychlorinated biphenyls. *J Adv Funct Mater.* 2012;22:218–24.
39. Li DY, He XW, Chen Y, Li WY, Zhang YK. Novel hybrid structure silica/CdTe/molecularly imprinted polymer: synthesis, specific recognition, and quantitative fluorescence detection of bovine hemoglobin. *J ACS Appl Mater Interfaces.* 2013;5:12609–16.
40. Chen Y, Donoghue MBO, Huang YF, Kang H, Phillips JA, Chen X, et al. A surface energy transfer nanoruler for measuring binding site distances on live cell surfaces. *J Am Chem Soc.* 2010;132:16559–70.
41. Yoshimi Y, Sato K, Ohshima M, Piletska E. Application of the “gate effect” of a molecularly imprinted polymer grafted on an electrode for the real-time sensing of heparin in blood. *J Analyst.* 2013;138: 5121–8.
42. Yoshimi Y, Narimatsu A, Nakayama K, Sekine S, Hattori K, Sakai K. Development of an enzyme-free glucose sensor using the gate effect of a molecularly imprinted polymer. *J Artif Organs.* 2009;12: 264–70.
43. Guo Y, Kang LL, Chen SN, Li X. High performance surface-enhanced Raman scattering from molecular imprinting polymer capsulated silver spheres. *Phys Chem Chem Phys.* 2015;17: 21343–7.